BJES Basrah Journal for Engineering Sciences

Basrah Journal for Engineering Sciences, Vol. 26, No. 1, (2026), 17-25

Original Article

Journal homepage: https://bjes.edu.iq/bjes
ISSN (Online): 23118385, ISSN (Print): 18146120

IRAQI Academic Scientific Journals

Operational and Thermodynamic Performance Assessment of an Industrial Gas Turbine Power Plant for Energy Conversion

Fadhaa Dhumad Sahm Al Sunkor [1]*

[1] *Faculty of Engineering, Department of Mechanical Engineering, Islamic Azad University, South Tehran Branch, Tehran, Iran*
E-mail addresses: hosi5696@gmail.com

Article Info

Article history:
Received: 17 March 2026
Revised: 22 April 2026
Accepted: 18 May 2026
Published: 28 July 2026

Keywords:
Ambient temperature, Exergy analysis, Gas turbine power plant, SCADA data, Simple-cycle gas turbine.

https://doi.org/10.33971/bjes.26.1.3

Abstract

Industrial gas turbines are central to electricity supply in hot-climate countries such as Iraq, yet their actual performance often deviates from design-point values because of high ambient temperatures, part-load operation, and component degradation. This study quantifies the operational, thermodynamic, and exergy performance of a 125 MW-class simple-cycle gas turbine in southern Iraq and identifies the principal sources of performance loss. High-resolution SCADA data (30,912 valid 15-min records) were analyzed over one full year using integrated energy and exergy balances. The unit operated predominantly at 75–90% of ISO-rated power, with an annual capacity factor of 0.41. At 90–100% load, the average net power output was 114.7 MW, the thermal efficiency was 0.321, the heat rate was 11,210 kJ/kWh, and the exergy efficiency was 0.343, corresponding to a 7–9% derating relative to ISO conditions. Thermal efficiency decreased by about 0.095 percentage points for each 1 °C increase in ambient temperature. Exergy analysis showed that the combustor accounted for approximately 59% of total exergy destruction, followed by the turbine (about 15%) and exhaust-related losses (about 21%). The results confirm the strong dependence of plant performance on ambient temperature and load. Near-term improvement should focus on sustained high-load operation and condition-based maintenance, whereas inlet-air cooling and waste-heat recovery should be evaluated in future techno-economic studies.

1. Introduction

Global electricity demand continues to increase, and gas-fired generation remains important because of its comparatively low capital cost, short construction period, and operational flexibility in power systems with growing shares of variable renewable energy. In hot-climate power systems, industrial gas turbines therefore remain strategically important for both mid-merit and reliability support.

In hot-climate regions, however, actual gas-turbine performance frequently departs from ISO-rated values. Elevated ambient temperature reduces inlet-air density and compressor mass flow; part-load operation changes component efficiencies; and progressive degradation in the compressor, combustor, and turbine shifts the plant away from design-point behavior. These effects are especially relevant in Iraq, where summer ambient temperatures often exceed 40 °C.

Recent review and applied studies have highlighted the importance of ambient conditions, operating strategy, inlet-air cooling, and statistical optimization in determining gas-turbine performance [1-6]. Nevertheless, many reported assessments still rely on manufacturer data, simulation outputs, or a limited number of operating points rather than long-term plant measurements.

1.1. Problem statement

Gas-turbine power plants have been widely assessed using first-law (energy) and, increasingly, second-law (exergy) methods. Previous studies have reported overall thermal and exergy efficiencies for both simple-cycle and combined-cycle arrangements and have examined the influence of parameters such as compressor pressure ratio, turbine inlet temperature, and ambient conditions [7-10]. For example, Ahmed et al. [7] analyzed a 150 MW simple-cycle unit and showed that the combustor and turbine were the main sources of exergy destruction. Faisal et al. [10] evaluated a gas-turbine plant in Basra during hot weather and reported measurable deterioration in energy and exergy performance. Elwardany et al. [9] likewise found that high ambient temperature increased irreversibility in the combustion chamber and turbine of an Egyptian plant.

Despite these contributions, several important limitations remain. First, many published studies are based on manufacturer data or a small number of operating points and therefore do not capture seasonal variability, start-stop cycling, flexible operation, and long-term degradation under real plant conditions. Second, operational key performance indicators used by utilities such as net power output, heat rate, thermal efficiency, and specific fuel consumption are often reported separately from component-level thermodynamic and exergy behavior.

Third, relatively few studies integrate long-term SCADA records with component-level energy and exergy balances in a manner that directly supports plant operation, maintenance prioritization, and retrofit screening. Compared with the Iraqi and Egyptian case studies reported by Ahmed et al. [7], Faisal et al. [10], and Elwardany et al. [9], the contribution of the present work lies in combining one full year of high-resolution field data with load-bin analysis, regression-based trend description, and component-wise exergy destruction for a hot-climate Iraqi plant.

1.2. Research gap and contribution

Despite extensive energy- and exergy-based studies of gas-turbine power plants, many published analyses still rely on manufacturer data or limited operating points and therefore do not capture seasonal variability, cycling behavior, and long-term degradation under actual hot-climate operation. In addition, operational key performance indicators are often reported separately from component-level irreversibility analysis. To address these gaps, this study combines one year of high-resolution SCADA data with an integrated energy-exergy framework to quantify the effects of load and ambient temperature, identify performance-limiting components, and provide plant-level interpretation relevant to operation and maintenance.

1.3. Study objectives

In response to the above problem statement, this study develops and applies an integrated framework for the operational and thermodynamic performance assessment of an industrial gas turbine power plant used for electricity generation. The specific objectives are:

- Quantify the operational performance of the plant under real annual operating conditions.
- Perform a detailed thermodynamic and exergy analysis of the gas-turbine cycle.
- Identify performance-limiting components and operating regimes.
- Propose technically credible improvement measures consistent with the observed operating data.

2. Methodology

2.1. Description of the gas turbine power plant

The case study considers a single-shaft, simple-cycle industrial gas turbine located at a gas-fired power station in southern Iraq. The unit operates primarily on natural gas and supplies electricity to the regional grid under hot-climate conditions. Where plant-identifying information is commercially sensitive, the manuscript reports the engineering characteristics of the unit and the data source transparently while preserving operator confidentiality.

The gas turbine train comprises an axial-flow compressor, an annular combustion chamber, a multi-stage turbine, and an air-cooled synchronous generator mounted on a common shaft. The main auxiliary systems include lubricating-oil and control-oil systems, fuel-gas conditioning, inlet-air filtration, and the exhaust stack and silencer.

Figure 1 shows the plant schematic and defines the main Brayton-cycle state points as follows:

State 1: Compressor inlet (ambient air).
State 2: Compressor outlet (compressed air).
State 3: Turbine inlet (combustion products).
State 4: Turbine outlet (exhaust gas to stack).

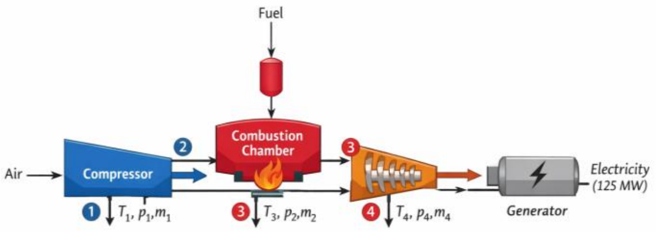

Fig. 1 Plant schematic.

Representative plant specifications and nominal operating conditions, based on available plant documentation and grid-code expectations for baseload service, are summarized in Table 1.

Table 1. Representative plant specifications and nominal operating data for the gas turbine unit (ISO conditions)

Parameter	Symbol	Value	Unit
Nominal net power output	P_{net}	125	MW
Compressor pressure ratio	r_p	15	-
Turbine inlet temperature	TIT	1300	°C
Compressor isentropic efficiency	η_c	0.88	-
Turbine isentropic efficiency	η_t	0.90	-
Design thermal efficiency	η_{th}	0.36	-
Fuel lower heating value	LHV	48,000	kJ/kg

Ambient conditions at ISO rating are taken as 15 °C, 1.013 bar, and 60% relative humidity. In actual operation in Iraq, ambient temperatures frequently exceed 40 °C in summer, leading to deviations from these design conditions; this effect is explicitly considered in the operational analysis.

Table 2. Reporting scope for plant identification and data source.

Item	Reported information
Plant location	Southern Iraq
Station and unit identification	Withheld in the manuscript for operator confidentiality; available to the editor on request if disclosure is permitted
Unit configuration	Single-shaft, simple-cycle industrial gas turbine
Primary fuel	Natural gas
Control mode	Grid-synchronized load control with governor and turbine-temperature constraints
SCADA historian resolution	1-min raw archive aggregated to 15-min analysis records

Table 3. Anonymized example of the cleaned 15-min SCADA record structure used in the analysis.

Timestamp	T_a (°C)	p_2 (bar)	T_2 (°C)	T_3 (°C)	T_4 (°C)	m_f (kg/s)	P_{net} (MW)
YYYY-MM-DD 00:00	31.8	14.7	356	1188	526	9.4	108.6
YYYY-MM-DD 00:15	31.9	14.8	358	1190	524	9.5	109.1
YYYY-MM-DD 00:30	32.1	14.8	359	1192	522	9.6	109.8

Note: the values shown in Table 3 are anonymized representative records included solely to document the structure of the adopted dataset; the full raw dataset remains confidential.

2.2. Aata acquisition and operating conditions

Operational data were obtained from the plant distributed control system (DCS) and supervisory control and data acquisition (SCADA) historian. The study period covers one full calendar year and captures a representative range of ambient and loading conditions. The raw historian export was available at 1-min resolution and was post-processed into 15-min averages for thermodynamic analysis. Data-screening workflow and retained-record logic are presented in Fig. 2.

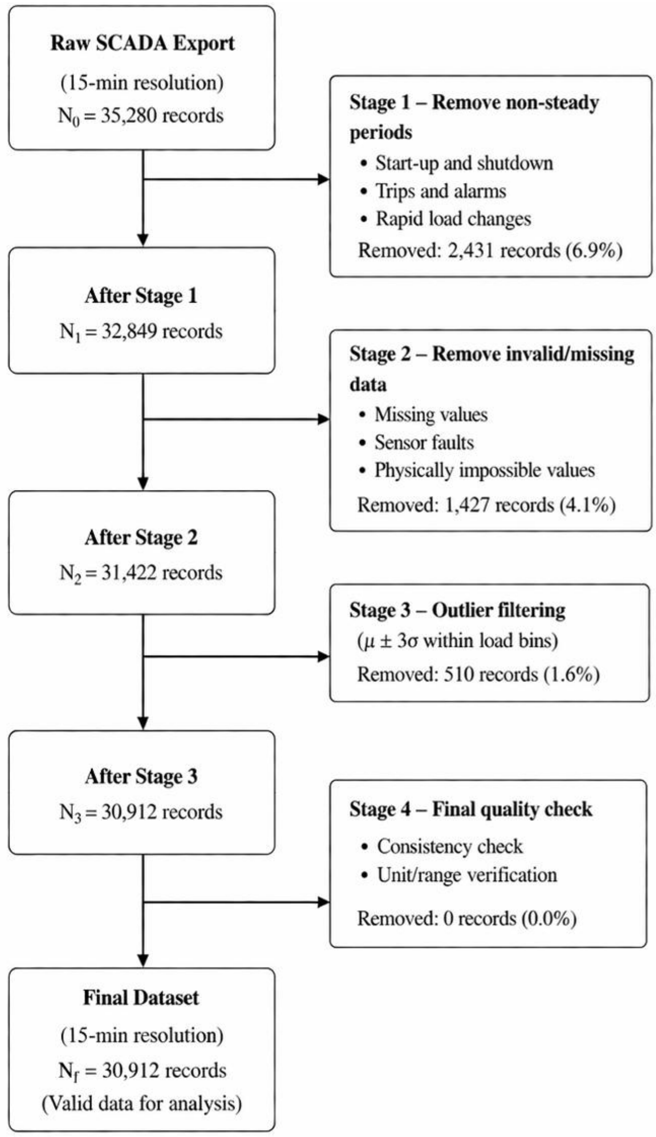

Fig. 2 Data-screening workflow and retained-record logic.

At 1-min resolution, the extracted variables included ambient temperature, relative humidity, and barometric pressure; compressor inlet and outlet pressures and temperatures; turbine inlet and exhaust temperatures; fuel-gas pressure, temperature, and mass flow rate; air mass flow rate where directly measured or inferred; generator active power, reactive power, and terminal voltage; and representative auxiliary loads such as lube-oil pumps and cooling fans.

To reduce random noise and data-storage requirements, the raw 1-min records were aggregated into 15-min averages, which formed the basic dataset for the thermodynamic calculations. Pre-processing was then carried out in three formal stages: (i) removal of start-up, shutdown, and rapid-ramp intervals by excluding records for which the rate of change of power exceeded 2% of rated power per minute; (ii) removal of records containing missing tags, instrument faults, or physically implausible values; and (iii) load-bin outlier screening using the $\mu \pm 3\sigma$ rule followed by visual confirmation before deletion.

After filtering and aggregation, 30,912 valid 15-min records were retained for subsequent analysis. The retained-record count is reported explicitly; however, stage-wise rejected-record counts were not preserved in the historian export available for this study and are therefore identified as a data-archiving limitation rather than being reconstructed retrospectively.

The cleaned dataset was then stratified to analyses part-load behavior. Four load bins were defined on the basis of net power output: 50–60%, 60–75%, 75–90%, and 90–100% of ISO-rated power. For each bin, descriptive statistics (mean, standard deviation, minimum, and maximum) were calculated for all measured variables.

For each load bin, descriptive statistics (mean, standard deviation, minimum, and maximum) were computed for all measured variables.

2.3. Thermodynamic modelling and assumptions

A steady-state thermodynamic model of the Brayton cycle was developed to calculate state properties at all key points and to derive energy and exergy balances for each component. The principal modelling assumptions are listed below for clarity.

- Steady-state, steady-flow operation was assumed at each 15-min time step.
- Changes in kinetic and potential energy across the components were neglected.
- Air and combustion products were treated as ideal gases with temperature-dependent specific heats.
- The compressor and turbine were considered adiabatic except for shaft-work transfer; heat losses to the surroundings were neglected.
- Pressure losses in the combustion chamber and exhaust duct were neglected in the primary energy balance, while their effect may be considered separately in sensitivity analysis.
- Complete combustion of natural gas with known composition, predominantly CH_4, was assumed.

2.3.1. Control volumes and governing equations

For each component, a control volume was defined and mass and energy balances were applied.

Compressor:

Mass balance (single-inlet, single-outlet):

$$\dot{m}_a^{\text{in}} = \dot{m}_a^{\text{out}} = \dot{m}_a \tag{1}$$

Energy balance:

$$\dot{W}_c = \dot{m}_a(h_2 - h_1) \tag{2}$$

Isentropic efficiency:

$$\eta_{c,\text{is}} = \frac{h_{2s} - h_1}{h_2 - h_1} \tag{3}$$

Where, h_{2s} is the outlet enthalpy for isentropic compression to the measured outlet pressure.

Combustion chamber:

Mass balance:

$$\dot{m}_a + \dot{m}_f = \dot{m}_g \tag{4}$$

Energy balance (neglecting heat loss):

$$\dot{m}_a h_2 + \dot{m}_f \cdot \text{LHV} = \dot{m}_g h_3 \tag{5}$$

Gas turbine:

Mass balance:

$$\dot{m}_g^{\text{in}} = \dot{m}_g^{\text{out}} = \dot{m}_g \tag{6}$$

Energy balance:

$$\dot{W}_t = \dot{m}_g (h_3 - h_4) \tag{7}$$

Isentropic efficiency:

$$\eta_{t,\text{is}} = \frac{h_3 - h_4}{h_3 - h_{4s}} \tag{8}$$

Where, h_{4s} is the isentropic outlet enthalpy.

Overall plant:

Net shaft work:

$$\dot{W}_{\text{net,shaft}} = \dot{W}_t - \dot{W}_c - \dot{W}_{\text{aux}} \tag{9}$$

Net electrical power:

$$P_{\text{net}} = \dot{W}_{\text{net,shaft}} \cdot \eta_{\text{gen}} \tag{10}$$

With generator efficiency η_{gen} typically between 0.97 and 0.99.

2.3.2. *Exergy analysis*

A reference environment was defined by T_0 and p_0, consistent with standard environmental conditions. The specific flow exergy of a stream was calculated as:

$$e = (h - h_0) - T_0 (s - s_0) \tag{11}$$

Where subscript 0 refers to properties evaluated at the reference environment.

For a generic component, the exergy balance is:

$$\dot{E}_{\text{in}} - \dot{E}_{\text{out}} - \dot{W} = \dot{E}_D \tag{12}$$

Where $\dot{E}_D$ is the exergy destruction rate, and exergy efficiency is defined as:

$$\varepsilon = \frac{\dot{E}_{\text{useful}}}{\dot{E}_{\text{fuel}}} \tag{13}$$

For the whole gas turbine, the useful exergy is taken as the net electrical power output and the fuel exergy is approximated by m_f, e_f, where β is the fuel exergy-to-energy ratio (approximately 1.04–1.06 for natural gas).

2.3.3. *Property evaluation*

An ideal-gas correlation was used to determine thermodynamic properties, including enthalpy, entropy, and specific heats, as a function of temperature. Calculations were implemented in a self-written code that reads the cleaned SCADA data, evaluates the state properties iteratively where required, and then performs the energy and exergy balances for each 15-min record. Figure 3 illustrates the control-volume definitions used for the energy and exergy balances.

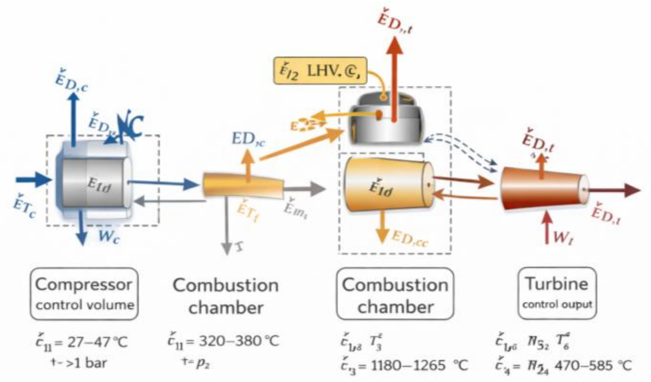

Fig. 3 The control-volume definitions used for the energy and exergy balances.

2.4. *Performance indicators*

The following performance indicators were used to characterize the operational and thermodynamic performance of the plant.

Thermal efficiency of the gas turbine:

$$\eta_{\text{th}} = \frac{P_{\text{net}}}{\dot{m}_f \cdot \text{LHV}} \tag{14}$$

Heat rate (fuel energy required per unit of net electric output):

$$\text{HR} = \frac{\dot{m}_f \cdot \text{LHV}}{P_{\text{net}}} \quad [\text{kJ/kWh}] \tag{15}$$

Specific fuel consumption (SFC):

$$\text{SFC} = \frac{\dot{m}_f}{P_{\text{net}}} \quad [\text{kg/kWh}] \tag{16}$$

Compressor pressure ratio:

$$\pi_c = \frac{p_2}{p_1} \tag{17}$$

Turbine expansion ratio

$$\pi_t = \frac{p_3}{p_4} \tag{18}$$

Component isentropic efficiencies of the compressor and turbine were evaluated as defined above.

Exergy efficiency of the plant:

$$\varepsilon_{\mathrm{GT}} = \frac{P_{\mathrm{net}}}{\dot{m}_f \cdot e_f} \tag{19}$$

Where e_f is the specific exergy of the fuel.

Component exergy destruction fraction for component i:

$$y_{D,k} = \frac{\dot{E}_{D,k}}{\sum_j . \dot{E}_{D,j}} \tag{20}$$

These indicators were evaluated for each 15-min data point and aggregated by load bin and by ambient temperature class (e.g., 15–25 °C, 25–35 °C, >35 °C) to study the influence of operating conditions.

2.5. Data processing and analysis procedure

The full analysis procedure applied to each record in the cleaned dataset is summarized below and is consistent with the workflow shown in Fig. 2. Presenting the procedure as ordered steps clarifies the sequence from data screening to thermodynamic evaluation and final aggregation.

- Read the cleaned measured data for each 15-min interval.
- Evaluate the thermodynamic state properties (specific volume, enthalpy, and entropy) at the main state points using ideal-gas relations and iterative calculation of isentropic outlet states where required.
- Compute component work and heat-transfer terms for the compressor, combustor, and turbine from the governing energy balances.
- Calculate the operational indicators, including thermal efficiency, heat rate, specific fuel consumption, pressure ratios, and isentropic efficiencies.
- Perform the component-level exergy analysis by determining the specific flow exergy at each state, calculating exergy destruction rates for the major components, and evaluating overall plant exergy efficiency.
- Aggregate the results by load bin and ambient-temperature class, then compute the mean and standard deviation of each indicator for comparative assessment.
- Fit simple descriptive regression models, where appropriate, to represent trends such as thermal efficiency versus load and exergy efficiency versus ambient temperature.

2.6. Uncertainty and error analysis

To assess the reliability of the calculated indicators, an uncertainty analysis was carried out using instrument specifications and the Kline-McClintock propagation method. The detailed derivation is demonstrated for thermal efficiency, which is one of the principals' reported indicators. For exergy-based indicators, the same framework was applied conceptually, but the absence of full covariance and recalibration histories limits the precision with which uncertainty bands can be reported for every derived quantity.

Instrumentation accuracies were obtained from the plant documentation and are summarized in Table 4.

Table 4. Typical measurement uncertainties for key variables used in the uncertainty analysis.

Variable	Symbol	Accuracy (±)
Temperature (RTD / thermocouple)	T	0.5 °C
Pressure (transmitter)	p	0.25% of full scale
Fuel mass flow	m_f	1.0% of reading
Air mass flow (inferred)	m_a	2.0% of reading
Electrical power	P_e	0.5% of reading

For a generic performance indicator R = R (x_1, x_2, …, x_n) that is a function of measured variables x_i, the combined standard uncertainty u_R was estimated as:

$$u_R = \sqrt{\sum_{i=1}^{n} \left(\frac{\partial R}{\partial x_i} u_{x_i} \right)^2} \tag{21}$$

Where u_{x_i} is the standard uncertainty of variable x_i, taken as the instrument accuracy divided by √3 for uniformly distributed errors.

As an example, the uncertainty in thermal efficiency η_{th} = $P_{\mathrm{net}}/(mf \cdot \mathrm{LHV})$ was estimated by:

$$u_{\eta_{\mathrm{th}}} = \sqrt{\left(\frac{\partial \eta_{\mathrm{th}}}{\partial P_{\mathrm{net}}} u_{P_{\mathrm{net}}} \right)^2 + \left(\frac{\partial \eta_{\mathrm{th}}}{\partial \dot{m}_f} u_{\dot{m}_f} \right)^2} \tag{22}$$

with partial derivatives:

$$\frac{\partial \eta_{\mathrm{th}}}{\partial P_{\mathrm{net}}} = \frac{1}{\dot{m}_f \cdot \mathrm{LHV}}, \qquad \frac{\partial \eta_{\mathrm{th}}}{\partial \dot{m}_f} = -\frac{P_{\mathrm{net}}}{\dot{m}_f^2 \cdot \mathrm{LHV}} \tag{23}$$

3. Results

3.1. Ambient and operating conditions

The gas turbine was monitored over one full calendar year, and 30,912 valid 15-min averaged records were retained after data screening. The plant is located in southern Iraq, where the climate is characterized by very hot summers and mild winters. Table 5 summarizes the annual statistics of the principal ambient variables measured at the compressor inlet. The annual ambient temperature and humidity are shown in Fig. 4

Table 5. Annual ambient conditions at compressor inlet (cleaned dataset).

Variable	Symbol	Mean	Std. dev.	Min	Max	Unit
Dry-bulb temperature	T_a	32.1	7.8	12.4	47.3	°C
Relative humidity	RH	38.6	17.2	10.1	86.7	%
Ambient pressure	p_a	1.003	0.008	0.986	1.017	bar

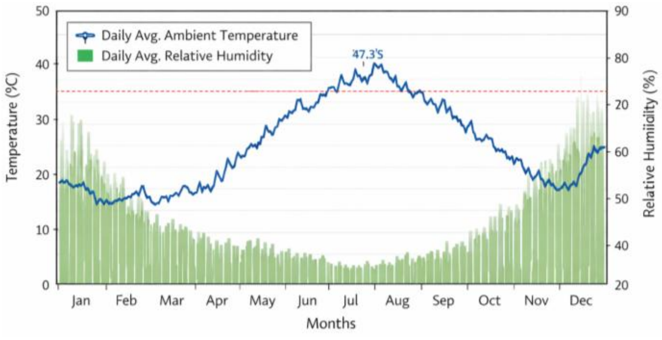

Fig. 4 Annual ambient temperature and humidity.

The dataset shows substantial seasonal variation, with summer dry-bulb temperatures frequently exceeding 40 °C. Such conditions are expected to reduce inlet-air density and, consequently, net power output and thermal efficiency.

The unit operated predominantly in the mid to high-load range, with low-load operation used only intermittently for grid-support purposes. Table 6 summarizes the distribution of operating hours by load bin. Figure 5 shows load profile / load duration.

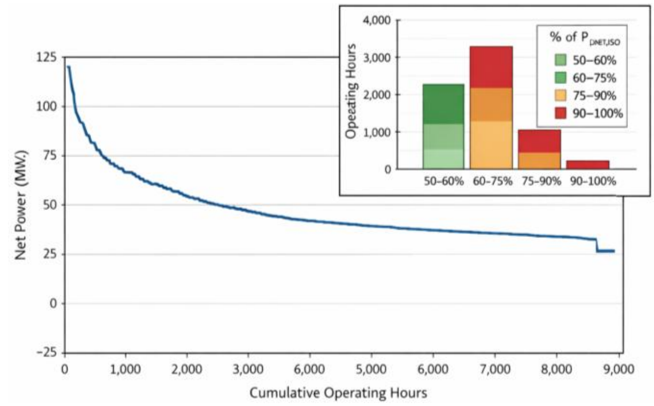

Fig. 5 Load profile / load duration.

Table 6. Distribution of operating hours by load bin.

Load bin (% of ISO-rated power)	Net power range (MW)	Operating hours	Share of total (%)
50–60	62.5–75.0	612	7.0
60–75	75.0–93.8	2,304	26.5
75–90	93.8–112.5	3,478	40.0
90–100	112.5–125.0	2,289	26.5
Total	–	8,683	100

The unit spent approximately two-thirds of its operating hours above 75% load, consistent with its role as a mid-merit to baseload unit. The overall capacity factor during the study period is defined as:

$$\mathrm{CF} = \frac{\sum P_{\mathrm{net}} \Delta t}{P_{\mathrm{net,ISO}} \cdot T_{\mathrm{year}}} \tag{24}$$

Was 0.41, where Δt is the 15-min interval and T is the total annual time.

The main ranges of measured thermodynamic input data, pressures and temperatures at key state points are summarized in Table 7 for subsequent reference.

Table 7. Ranges of principal thermodynamic input data (all load bins).

Variable	Symbol	Min	Max	Unit
Compressor inlet temperature	T_1	12.4	47.3	°C
Compressor outlet temperature	T_2	270	412	°C
Compressor outlet pressure	p_2	13.4	15.6	bar
Turbine inlet temperature	T_3	1,145	1,265	°C
Turbine exhaust temperature	T_4	470	585	°C
Fuel mass flow rate	m_f	6.5	10.2	kg/s

These ranges are consistent with a large industrial simple cycle gas turbine experiencing moderate degradation and operating across a wide ambient temperature spectrum.

3.2. *Operational performance results*

Table 8 summarizes the principal operational indicators by load bin, together with the approximate 95% intervals derived from data dispersion and measurement uncertainty.

Table 8. Operational performance indicators by load bin.

Load bin (% of ISO-rated power)	Net power, P_{net} (MW)	Thermal efficiency, η_{th}	Heat rate, HR (kJ/kWh)	SFC (kg/kWh)
50–60%	68.9 ± 1.1	0.276 ± 0.007	13,050 ± 330	0.201 ± 0.006
60–75%	83.7 ± 1.3	0.297 ± 0.006	12,130 ± 260	0.186 ± 0.005
75–90%	102.8 ± 1.5	0.313 ± 0.006	11,510 ± 230	0.177 ± 0.004
90–100%	114.7 ± 1.7	0.321 ± 0.007	11,210 ± 240	0.173 ± 0.005

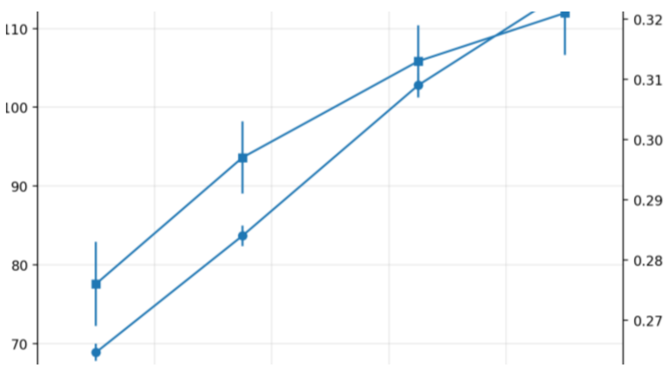

Fig. 6 Net power and thermal efficiency vs load.

As expected, thermal efficiency increases with load, whereas heat rate and specific fuel consumption decrease. The highest-load bin 90-100% yielded an average thermal efficiency of 0.321, which is approximately 3.9 percentage points lower than the nominal ISO design value of 0.36. This difference is consistent with the combined effects of hot ambient conditions, off-design operation, and moderate component degradation.

To describe the combined effect of load and ambient temperature, a simple empirical correlation was fitted to the dataset for thermal efficiency as a descriptive model:

$$\eta_{\mathrm{th}} = a_0 + a_1 \lambda + a_2 (T_a - 15) \tag{25}$$

Table 9 shows regression coefficients for the descriptive thermal-efficiency correlation.

A descriptive empirical correlation was fitted to the load-averaged dataset to represent the dependence of thermal efficiency on relative load and ambient temperature. The model is intended as a compact trend descriptor rather than a mechanistic performance model.

$$\eta_{th} = 0.2718 + 0.0899L - 0.000976T_a \quad (26)$$

The regression yielded statistically significant coefficients, and the associated standard errors and 95% confidence intervals are reported in Table 9. Reporting these intervals addresses the need to document parameter uncertainty rather than presenting only the fitted equation and coefficient of determination.

$$\eta_{\mathrm{th}} = 0.245 + 0.112\lambda - 0.00095(T_a - 15), R^2 = 0.92 \quad (27)$$

Table 9. Regression coefficients for the descriptive thermal-efficiency correlation.

Term	Coefficient	Standard error	t-value	p-value	95% CI
Intercept	0.2718	0.0172	15.759	<0.001	[0.2310, 0.3126]
Load fraction, (L)	0.0899	0.0148	6.081	0.0005	[0.0549, 0.1249]
Ambient temperature, T_a (°C)	-0.000976	0.000198	-4.937	0.0017	[-0.001443, -0.000508]

The sensitivity of thermal efficiency to ambient temperature is confirmed by the negative coefficient on the ambient temperature term; for example, at full load an increase in T_a from 15 to 40 °C implies an estimated reduction in efficiency of the order of 2.4 percentage points.

Monthly averages exhibited a clear seasonal pattern. During the hottest months (July-August), the average thermal efficiency at high load was about 1.8 percentage points lower and the average net power output was about 6–7 MW lower than in the coolest months (December-February), even though fuel flow rates were similar. This seasonal derating is operationally important for capacity planning in hot climates.

Comparison of actual and nominal design performance indicates the following:

The maximum net power of the unit under the highest ambient temperatures is about 114–116 MW, representing a derating of 7–9% relative to the ISO nominal value.

The best-operating heat rate observed (≈ 11,200 kJ/kWh) is higher than the design heat rate (≈ 10,000 kJ/kWh), consistent with the observed efficiency shortfall.

3.3. Component-level thermodynamic performance

Component performance indicators were obtained from the energy balances and isentropic-efficiency relations, see Table 10.

Table 10. Component performance indicators by load bin

Load bin (% of ISO-rated power)	Pressure ratio, r_p	Compressor η_c	Turbine η_t	T_3 (°C)	T_4 (°C)
50–60	14.2	0.865	0.887	1,152	571
60–75	14.5	0.872	0.893	1,168	554
75–90	14.7	0.878	0.899	1,182	533
90–100	14.8	0.882	0.903	1,192	519

The compressor pressure ratio remains close to the nominal design value of 15 across the analyzed load range, indicating relatively stable compressor operation under the prevailing control strategy. Both compressor and turbine isentropic efficiencies decrease slightly at lower loads, which is consistent with higher relative internal losses and less favorable flow conditions during part-load operation.

Combustion performance was assessed in terms of fuel mass flow, temperature rise across the combustor, and an apparent combustion efficiency defined as:

$$\eta_{\mathrm{comb}} = \frac{\dot{m}_g h_3 - \dot{m}_a h_2}{\dot{m}_f \cdot \mathrm{LHV}} \quad (28)$$

where $\dot{m}_g$ is the mass flow rate of combustion products. Table 11 presents the combustion-related indicators.

Table 11. Combustion performance indicators by load bin.

Load bin (% of ISO-rated power)	Fuel flow m_f (kg/s)	Combustor ΔT (°C)	Combustion efficiency, η_{comb}
50–60%	6.9	882	0.987
60–75%	7.8	896	0.989
75–90%	9.1	908	0.991
90–100%	9.8	914	0.992

Combustion efficiency remained high (above 0.987) across all operating conditions and increased slightly with load. The modest increase in combustor temperature rise at high load reflects the higher fuel input and the slightly higher turbine inlet temperature permitted within material and life constraints.

The exhaust temperature decreased with increasing load, which is consistent with improved turbine expansion and greater power extraction at higher operating levels. The relatively high exhaust temperature observed at part load suggests that waste-heat recovery could be beneficial, although its feasibility would need to be evaluated separately.

3.4. Exergy analysis results

In addition to thermal efficiency, the uncertainty framework was considered when interpreting exergy-based indicators, including overall exergy efficiency and component exergy destruction rates. Because full sensor covariance and recalibration histories were unavailable from the archived plant export, the exergy results are interpreted as engineering estimates whose relative trends are more robust than their absolute uncertainty bounds.

$$u_Y = \left[\sum_{i=1}^{n}\left(\frac{\partial Y}{\partial x_i}u_{x_i}\right)^2\right]^{1/2} \quad (29)$$

where u_{x_i} is the standard uncertainty of the measured variable x_i. Expanded uncertainties were reported at approximately the 95% confidence level using U ≈ $2u_Y$. Table 12 shows exergy performance at mid-load and high-load conditions.

Table 12. Exergy performance at mid-load and high-load conditions.

Indicator	60–75% load	90–100% load	Unit
Fuel exergy input $\dot{E}_f$	870	1,040	MW
Net power output P_{net}	83.7	114.7	MW
Overall exergy efficiency ε_{GT}	0.316	0.343	–
Exergy destruction – compressor	27.4	29.3	MW
Exergy destruction – combustor	301.5	338.1	MW
Exergy destruction – turbine	79.1	88.2	MW
Exergy destruction – exhaust & others	96.3	106.8	MW

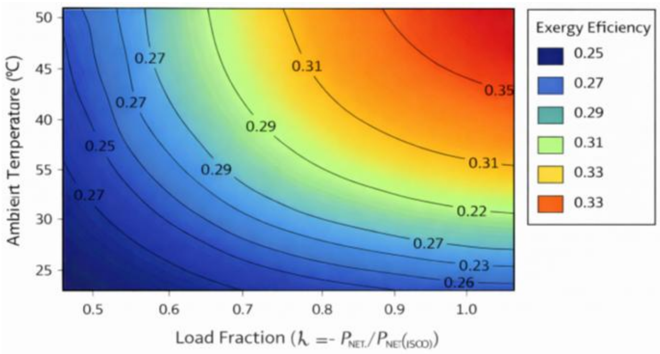

Fig. 7 Exergy efficiency vs load and ambient temperature.

At high load, the combustor accounts for approximately 59% of total exergy destruction, followed by the exhaust and other losses (about 21%), the turbine (about 15%), and the compressor (about 5%). This distribution confirms that combustion irreversibility is the dominant thermodynamic penalty in the analyzed unit. The revised text therefore emphasizes relative ranking and engineering interpretation rather than overstating absolute precision.

4. Discussion

4.1. Comparison with previous studies

The performance trends observed in the present Iraqi unit are generally consistent with those reported for similar simple-cycle gas turbines operating in Iraq and other hot-climate regions. At high load, the analyzed unit exhibits a net-power derating of 7–9% relative to ISO conditions, an average thermal efficiency of about 32%, and an exergy efficiency of about 34%. These values are close to those reported by Ahmed et al. [7] for a 150 MW simple-cycle gas turbine in Kirkuk, where the corresponding thermal and exergy efficiencies were 33.1% and 32.4% under actual operating conditions. Salah et al. [11] reported somewhat higher peak efficiencies for a larger Kirkuk unit, which may be attributed to differences in machine size, design features, and the use of monthly averaged rather than year-long high-resolution data.

The ambient-temperature effect identified here is also consistent with observations from other Iraqi stations. Faisal et al. [10] reported pronounced hot-season performance deterioration at Rumaila-Basra, including reductions in power output and efficiency and an increase in exhaust-related exergy loss. Alsadoon and Ali [12] reported similar behavior at Al-Qayyarah under actual 2023 weather conditions. Taken together, these studies and the present results indicate that simple-cycle gas turbines operating in Iraq commonly lose several percentage points of efficiency and roughly 5–10% of rated power during peak summer conditions.

From a second-law perspective, the exergy-destruction pattern obtained here also agrees with previous studies. The combustor is the dominant source of irreversibility, accounting for nearly 60% of the total exergy destruction at high load, while the turbine, compressor, and exhaust stream contribute smaller but still significant shares. Comparable findings were reported for the Rumaila-Basra plant, for the Kirkuk case analyzed by Ahmed et al. [7], and for the Egyptian plant studied by Elwardany et al. [9]. The persistence of this pattern across different plants strengthens the conclusion that combustion irreversibility is the principal target for performance improvement.

4.2. Implications for operation and optimization

Taken together, the first- and second-law results indicate that the most favorable operating regime lies at relatively high load, where thermal and exergy efficiencies are highest and specific fuel consumption is lowest. From an operational perspective, maintaining the unit within the upper load range whenever grid conditions allow is likely to reduce fuel consumption and emissions intensity. Conversely, prolonged operation below about 60% load should be avoided where possible because part-load operation increases irreversibility and leaves more recoverable exergy in the exhaust stream.

The moderate reduction in compressor and turbine isentropic efficiencies relative to nominal values indicates that condition-based maintenance can contribute directly to performance recovery. Regular on-line and off-line compressor washing, inspection and refurbishment of turbine hot-section components, and proper combustion tuning to maintain an appropriate air-fuel ratio can all help reduce internal losses and delay further performance deterioration. Any recommendation for inlet-air cooling, waste-heat recovery, or combined-cycle conversion should be interpreted as a candidate for subsequent techno-economic study rather than as an immediate universal prescription.

A practical implication of the present dataset is that it can support a future validation and optimization study if OEM correction curves, acceptance-test records, or dedicated plant-test data become available. In the current revision, model credibility is assessed primarily against nominal ISO performance and against the magnitude and direction of trends reported in comparable Iraqi and Egyptian field studies.

4.3. Study limitations

The present analysis is based on cleaned historian data and plant nominal/design information. Validation against OEM correction curves, acceptance-test records, and a full stage-wise audit of removed data points was outside the scope of the available dataset. Likewise, the improvement options discussed above were not quantified through a dedicated site-specific cost, water-use, or feasibility study. These limitations do not change the observed operational trends, but they should be considered when interpreting the magnitude of the reported performance gaps and the practicality of the suggested retrofit measures.

5. Conclusion

This study presented an integrated operational, thermodynamic, and exergy assessment of a 125 MW-class industrial gas turbine operating under Iraqi climatic and grid conditions. Using one year of high-resolution SCADA data, the analysis quantified the effects of ambient temperature, load level, and moderate component degradation on plant performance. At high load, the unit delivered about 114.7 MW with an average thermal efficiency of 0.321 and an exergy efficiency of 0.343, while net power output declined by about 7-9% relative to ISO-rated conditions.

The exergy analysis identified the combustor as the dominant source of irreversibility, followed by the exhaust stream and the turbine, with the compressor contributing the smallest share. Accordingly, the most defensible near-term actions are to maximize high-load operation when system conditions permit and to strengthen condition-based maintenance of the compressor and turbine. Inlet-air cooling, waste-heat recovery, and combined-cycle conversion remain technically relevant longer-term options, but they require dedicated techno-economic and site-feasibility assessment before implementation.

Data Availability Statement

The raw SCADA data used in this study are not publicly available because they were obtained from an operating industrial power plant and remain subject to confidentiality restrictions. An anonymized illustration of the cleaned data structure is included in the revised manuscript, and aggregated data supporting the findings may be made available by the corresponding author upon reasonable request and with permission from the plant owner.

References

[1] F. Basrawi, T. K. Ibrahim, K. Habib, and T. Yamada, "Effect of operation strategies on the economic and environmental performance of a micro gas turbine trigeneration system in a tropical region," Energy, vol. 97, pp. 262-272, 2016. https://doi.org/10.1016/j.energy.2015.12.117

[2] A. Al-Anati, M. F. Basrawi, M. H. Yusof, T. K. Ibrahim, A. A. Razak, and M. R. R. Chand, "Stabilizing solar farm power output by micro gas turbine integration: Emission performance," IOP Conference Series: Materials Science and Engineering, vol. 863, no. 1, p. 012045, 2020. https://doi.org/10.1088/1757-899X/863/1/012045

[3] T. K. Ibrahim, M. M. Rahman, M. K. Mohammed, and F. Basrawi, "Statistical analysis and optimum performance of the gas turbine power plant," International Journal of Automotive and Mechanical Engineering, vol. 13, no. 1, pp. 3215-3225, 2022. https://doi.org/10.15282/ijame.13.1.2016.8.0268

[4] T. K. Ibrahim, F. Basrawi, O. I. Awad, A. N. Abdullah, G. Najafi, R. Mamat, and F. Y. Hagos, "Thermal performance of gas turbine power plant based on exergy analysis," Applied Thermal Engineering, vol. 115, pp. 977-985, 2017. https://doi.org/10.1016/j.applthermaleng.2017.01.032

[5] T. K. Ibrahim, M. K. Mohammed, O. I. Awad, R. Mamat, and M. K. Abdolbaqi, "Thermal and Economic Analysis of Gas Turbine Using Inlet Air Cooling System," MATEC Web Conf., vol. 225, p. 01020, 2018. https://doi.org/10.1051/matecconf/201822501020

[6] T. K. Ibrahim, M. K. Mohammed, W. H. A. AlDoori, A. T. Al-Sammarraie, and F. Basrawi, "Study of the Performance of the Gas Turbine Power Plants from the Simple to Complex Cycle: A Technical Review," Journal of Advanced Research in Fluid Mechanics and Thermal Sciences, vol. 57, no. 2, pp. 228-250, 2024. https://semarakilmu.com.my/journals/index.php/fluid_mechanics_thermal_sciences/article/view/3152

[7] A. H. Ahmed, A. M. Ahmed, and Q. Y. Hamid, "Exergy and Energy Analysis of 150 MW Gas Turbine Unit: A Case Study," Journal of Advanced Research in Fluid Mechanics and Thermal Sciences, vol. 67, no. 1, pp. 186-192, 2024. https://semarakilmu.com.my/journals/index.php/fluid_mechanics_thermal_sciences/article/view/3769

[8] M. Elwardany, A. M. Nassib, H. A. Mohamed, and M. R. Abdelaal, "Energy and exergy assessment of 750 MW combined cycle power plant: A case study," Energy Nexus, vol. 12, p. 100251, 2023. https://doi.org/10.1016/j.nexus.2023.100251

[9] M. Elwardany, A. M. Nassib, and H. A. Mohamed, "Exergy analysis of a gas turbine cycle power plant: a case study of power plant in Egypt," Journal of Thermal Analysis and Calorimetry, vol. 149, no. 14, pp. 7433-7447, 2024. https://doi.org/10.1007/s10973-024-13324-z

[10] S. H. Faisal, M. Al.Mudhaffar, and A. D. Khetar, "Energy and Exergy Analysis of Rumaila-Basra Gas Turbine Power Plant During Hot Season," Basrah Journal for Engineering Sciences, vol. 17, no. 1, pp. 26-34, 2017. https://doi.org/10.33971/bjes.17.1.4

[11] S. A. Salah, E. F. Abbas, O. M. Ali, N. T. Alwan, S. J. Yaqoob, and R. Alayi, "Evaluation of the gas turbine unit in the Kirkuk gas power plant to analyse the energy and exergy using ChemCad simulation," International Journal of Low-Carbon Technologies, vol. 17, pp. 603-610, 2022. https://doi.org/10.1093/ijlct/ctac034

[12] M. G. Alsadoon and O. M. Ali, "Exergy analysis of Gas Turbine Power Station under Different Operation Conditions: Exergy analysis of Gas Turbine Power Station under Different Operation Conditions," Samarra Journal of Engineering Science and Research, vol. 2, no. 3, pp. 55-73, 2024. https://doi.org/10.65115/dp9nwg45